IBRO Reports 9 (2020) 147–156

Contents lists available at ScienceDirect

IBRO Reports

journal homepage: www.elsevier.com/locate/ibror

Research Paper

The GluN3 subunit regulates ion selectivity within native N-methyl-D-aspartate receptors

Stephen Beesley, Thomas Sullenberger, Sanjay S. Kumar*

Department of Biomedical Sciences, College of Medicine & Program in Neuroscience, Florida State University, 1115 W. Call Street, Tallahassee, FL 32306-4300, United States

ARTICLE INFO

Keywords:
Triheteromeric NMDA receptors
GluN3
Ion selectivity
Entorhinal cortex
Somatosensory cortex
Ion-substitution experiments
Electrophysiology

ABSTRACT

Glutamatergic N-methyl-D-aspartate receptors (NMDARs) are heterotetrameric proteins whose subunits are derived from three gene families, GRIN1 (codes for GluN1), GRIN2 (GluN2) and GRIN3 (GluN3). In addition to providing binding sites for glutamate and the co-agonist glycine, these subunits in their di (*d*-) and tri (*t*-) heteromeric configurations regulate various aspects of receptor function in the brain. For example, the decay kinetics of NMDAR-mediated synaptic currents depend on the type of GluN2 subunit (GluN2A-GluN2D) in the receptor subunit composition. While much is known about the contributions of GluN1 and GluN2 to *d*-NMDAR function, we know comparatively little about how GluN3 influences the function of *t*-NMDARs composed of one or more subunits from each of the three gene families. We report here that in addition to altering kinetics and voltage-dependent properties, the GluN3 subunit endows these receptors with ion selectivity wherein influx of Ca^{2+} is preferred over Na^{+}. This became apparent in the process of assessing Ca^{2+} permeability through these receptors and is of significance given that NMDARs are generally believed to be nonselective to cations and increased selectivity can lead to enhanced permeability. This was true of two independent brain regions where *t*-NMDARs are expressed, the somatosensory cortex, where both receptor subtypes are expressed at separate inputs onto single neurons, and the entorhinal cortex, where they are co-expressed at individual synaptic inputs. Based on this data and the sequence of amino acids lining selectivity filters within these subunits, we propose GluN3 to be a regulatory subunit for ion selectivity in *t*-NMDARs.

Introduction

NMDARs are implicated in a wide variety of Ca^{2+}-dependent cellular processes in the brain – normal and pathological – ranging from synaptic plasticity, the basis of learning and memory, to excitotoxicity and cell death (Collingridge, 1987; Cull-Candy et al., 2001; McBain and Mayer, 1994; Sheng et al., 1994). All NMDARs contain one or more of the obligatory glycine-binding GluN1 subunits, which when assembled with glutamate-binding GluN2 (GluN2A-GluN2D) subunits of the same type, give rise to conventional diheteromeric NMDARs (*d*-NMDARs). Triheteromeric NMDARs, on the other hand, contain three different types of subunits (Chazot and Stephenson, 1997; Hatton and Paoletti, 2005; Kumar and Huguenard, 2003; Luo et al., 1997; Mayer et al., 1984; Sheng et al., 1994; Tovar et al., 2013), and include receptors that are composed of one or more subunits from each of the three gene families, notably the glycine-binding GluN3 subunit, designated *t*-NMDARs (Beesley et al., 2019; Kumar, 2016; Pilli and Kumar, 2012, 2014).

These glutamate-activated, voltage-dependent ionotropic channels are Ca^{2+} permeable and widely believed to be nonselective to cations (Dingledine et al., 1999; Moriyoshi et al., 1991). Lack of selectivity is however not the default state because ion channels are inherently highly selective for an ion species and single amino acid substitutions within their selectivity filters can drastically alter their ion-selective properties. Asparagine residues at homologous locations within the pore-forming transmembrane 2 (TM2) domains of proteins that constitute the selectivity filter are therefore conserved in all members of the GluN1 and GluN2 subunit families enabling *d*-NMDARs to select for both Na^{+} and Ca^{2+} ions (Burnashev et al., 1992a; Verdoorn et al., 1991). However, the consequences of incorporating GluN3, a subunit in which the asparagine is replaced with glycine, on cation selectivity of *t*-NMDARs have not been elucidated. Here, we show that a triheteromeric assembly of GluN1, GluN2 and GluN3 subunits can render native synaptic NMDARs selective for Ca^{2+} over Na^{+}, in contrast with receptors

* Corresponding author at: Department of Biomedical Sciences, College of Medicine, Suite 3300-B, Florida State University, 1115 West Call Street, Tallahassee, FL 32306-4300, United States.
E-mail address: sanjay.kumar@med.fsu.edu (S.S. Kumar).

https://doi.org/10.1016/j.ibror.2020.07.009
Received 16 May 2020; Accepted 17 July 2020

assembled with just GluN1 and GluN3 subunits that exhibit the opposite trend (Das et al., 1998; Matsuda et al., 2002).

We chose the entorhinal and somatosensory cortices in brain tissue to assay for differences in Ca^{2+} permeability through these receptors owing to the inherent difficulty of stably expressing *t*-NMDARs using expression systems without precluding the co-expression of *d*-NMDARs (Cummings et al., 2017; Sun et al., 2017). Furthermore, we believe that artificially reconstituted NMDARs may be functionally distinct from those native to brain tissue. The areas chosen have been used in our previous studies to isolate and characterize *t*-NMDARs at *synapses*, to delineate them from *d*-NMDARs at the same or separate synaptic inputs onto neurons in intact brain slices, and to assay their subunit stoichiometry using a combination of approaches including electrophysiology, pharmacology and cell biology (Beesley et al., 2019; Pilli and Kumar, 2012, 2014). Our data suggests that permeation of Na^+ and Ca^{2+} through *t*-NMDAR channels in these areas is governed by cation selectivity with the GluN3 subunit as a *regulatory* element. Furthermore, we show that increased selectivity for Ca^{2+} in these receptors underlies their increased permeability to it compared with *d*-NMDARs. Thus, GluN3-containing *t*-NMDARs and GluN2-containing *d*-NMDARs may belong to a spectrum of receptor channels with variable levels of Ca^{2+} selectivity relative to Na^+ wherein the schema for ion selectivity in non-ligand gated ion channels seems to have carried over to ligand-gated channels despite differences in the make-up of their selectivity filters. Subunit-dependent cation selectivity represents a hitherto unrealized mechanism for finer control of Ca^{2+} influx that further enhances the repertoire of synaptic NMDARs.

Experimental procedures

All experiments were carried out in accordance with the National Institutes of Health *Guide for the Care and Use of Laboratory Animals* and were approved by the Florida State University Institutional Animal Care and Use Committee.

Electrophysiological recording

Electrophysiology was carried out in acute thalamocortical and entorhinal cortical slices cut from brains of adult male Sprague Dawley rats as described before in detail (Kumar and Buckmaster, 2006; Pilli and Kumar, 2012). Slices equilibrated in oxygenated (95 % O_2/5% CO_2) aCSF (in mM: 126 NaCl, 26 $NaHCO_3$, 3 KCl, 1.25 NaH_2PO_4, 2 $MgSO_4$, 2 $CaCl_2$, and 10 D-glucose, pH 7.4), first at 32 °C for 1 h and subsequently at room temperature (RT) before being transferred to the recording chamber. Whole-cell patch clamp recordings (Multiclamp 700B amplifier / pClamp, Molecular Devices) were made from excitatory pyramidal neurons at 32 °C with electrodes (1.2–2 μm tip diameters; 3 − 6 MΩ) containing the following (in mM) 120 cesium gluconate, 1 $MgCl_2$, 1 $CaCl_2$, 11 CsCl, 10 HEPES, 2 NaATP, 0.3 NaGTP, 1 QX-314, 11 EGTA, and 20 biocytin (pH 7.3 was corrected with Cs-OH, 290 mOsm). Stimulating electrodes (CE-2C75 and/or CB-ARC75, FHC) delivered constant current pulses 50 μs in duration and 1–50 mA in amplitude at low frequencies (0.1 − 0.3 Hz) to activate distinct pathways. A minimal stimulation paradigm was used to evoke single-fiber responses (Kumar and Huguenard, 2003) that consisted of increasing current intensity until postsynaptic responses could be evoked and were held constant at ~1.2 times threshold. Series resistance was monitored continuously, and cells in which this parameter exceeded 15 MΩ or changed by > 20 % were rejected. Series resistance compensation was not used. Current-voltage relationships, obtained by changing membrane potential according to a predetermined randomized sequence, are presented as ensemble averages of EPSC amplitudes normalized to their respective values at -84 mV (corrected for liquid junction potential) for each cell in a group (Beesley et al., 2019), irrespective of the shape of their *I–Vs*. Normalizing responses at potentials close to rest precluded distortions in the directionality of the currents recorded at various holding potentials (Kumar, 2016). AMPA and NMDA receptor-mediated EPSCs were isolated pharmacologically using bath / local perfusion of a cocktail in aCSF containing (in μM) 50 picrotoxin and either 40 D-AP5, 0.1 NBQX (for AMPA) or, 10 NBQX (for NMDA).

Ion substitution experiments done at RT were used to assess Ca^{2+} permeability through NMDARs (Kumar et al., 2002; Pilli and Kumar, 2012). High-Ca^{2+} solutions were applied either via the bath or local perfusion system that enabled fast exchange of media at the level of the synapse (Kumar et al., 2002). Sections were maintained in oxygenated (100 %) HEPES-buffered Ringer's solution comprising (in mM): 135 NaCl, 2.5 KCl, 1 $MgCl_2$, 10 HEPES, and 1.8 $CaCl_2$, pH adjusted with NaOH to 7.4 and osmolarity with sucrose to 290 mOsm. Picrotoxin and NBQX (50 and 10 μM respectively) were added to the 1.8 (control), 10, and 20 mM Ca^{2+} solutions which were identical in composition to the bathing media except for $CaCl_2$ and NaCl concentrations which varied as (in mM): 1.8 and 135, 10 and 122.7, and 20 and 107.7, respectively. Reversal potentials (E_{rev}) were estimated from *I–V* relationships by linear interpolation of data points within ± 20 mV of where EPSCs changed polarity. Permeability ratios were computed using ionic activities instead of concentrations. Activity coefficients (γ) for various ions were computed (Kumar et al., 2002; Mayer and Westbrook, 1987; Pitzer and Mayorga, 1973). The respective γ values estimated for Na^+, K^+, and Ca^{2+} for the different Ca^{2+} solutions were as follows: 1.8 mM Ca^{2+}, 0.75, 0.71, and 0.298; 10 mM Ca^{2+}, 0.74, 0.69, and 0.295; and 20 mM Ca^{2+}, 0.72, 0.69, and 0.29. γ for the Cs^+-based internal solution ($[Cs^+]_i$ = 131 mM) was 0.72. Final ionic activity for solutions was computed as the product of γ and the corresponding molar concentration (Pilli and Kumar, 2012). The permeability of Ca^{2+} ($P_{Ca}{}^{2+}$) and Na^+ ($P_{Na}{}^+$) relative to Cs^+ ($P_{Cs}{}^+$ / $P_K{}^+$ assumed 1) was estimated from a nonlinear least-squares fit (using the Levenberg-Marquardt algorithm; Origin V6.0, Microcal Software, Northampton, MA) of E_{rev} of the NMDA receptor-mediated EPSCs (as a function of Ca^{2+} activity) to the extended constant-field Goldman–Hodgkin–Katz (GHK) equation (Mayer and Westbrook, 1987):

$$E_{rev} = \frac{RT}{F}\ln\frac{-b + (b^2 - 4ac)^{\frac{1}{2}}}{2a}$$

in which,

$$a = [Cs^+]_i + 4\frac{P_{Ca^{2+}}}{P_{Cs^+}}[Ca^{2+}]_i + \frac{P_{Na^+}}{P_{Cs^+}}[Na^+]_i$$

$$b = ([Cs^+]_i - [K^+]_o) + \frac{P_{Na^+}}{P_{Cs^+}}([Na^+]_i - [Na^+]_o)$$

$$c = -[K^+]_o - \frac{P_{Na^+}}{P_{Cs^+}}[Na^+]_o - 4\frac{P_{Ca^{2+}}}{P_{Cs^+}}[Ca^{2+}]_o$$

and F (9.648×10^4 C/mol) is the Faraday constant, z (+2) is the valence, R (8.315 J K^{-1} mol^{-1}) is the gas constant, and T (32 °C/305.2°K) is the temperature.

Sequence data: The amino acid sequences near the second transmembrane (TM2) segments of NMDA receptor subunits were obtained from the NCBI protein data base using accession numbers: NP_001257531.1, [RN] GluN1; NP_036705.3, [RN] GluN2A; NP_036706.1, [RN] GluN2B; Q00961.1, [RN] GluN2C; NP_073634.1, [RN] GluN2D; Q9R1M7.1, [RN] GluN3A; Q8VHN2.2, [RN] GluN3B. The sequences were aligned using *ClustW2* multiple sequence alignment computer program (EMBL-EBI).

Results

The data for Fig. 1 and portions of Fig. 2 was obtained from earlier studies (Beesley et al., 2019; Pilli and Kumar, 2012) and are being presented here to showcase the differences and/or similarities between *t*-NMDAR properties between the somatosensory and entorhinal cortices.

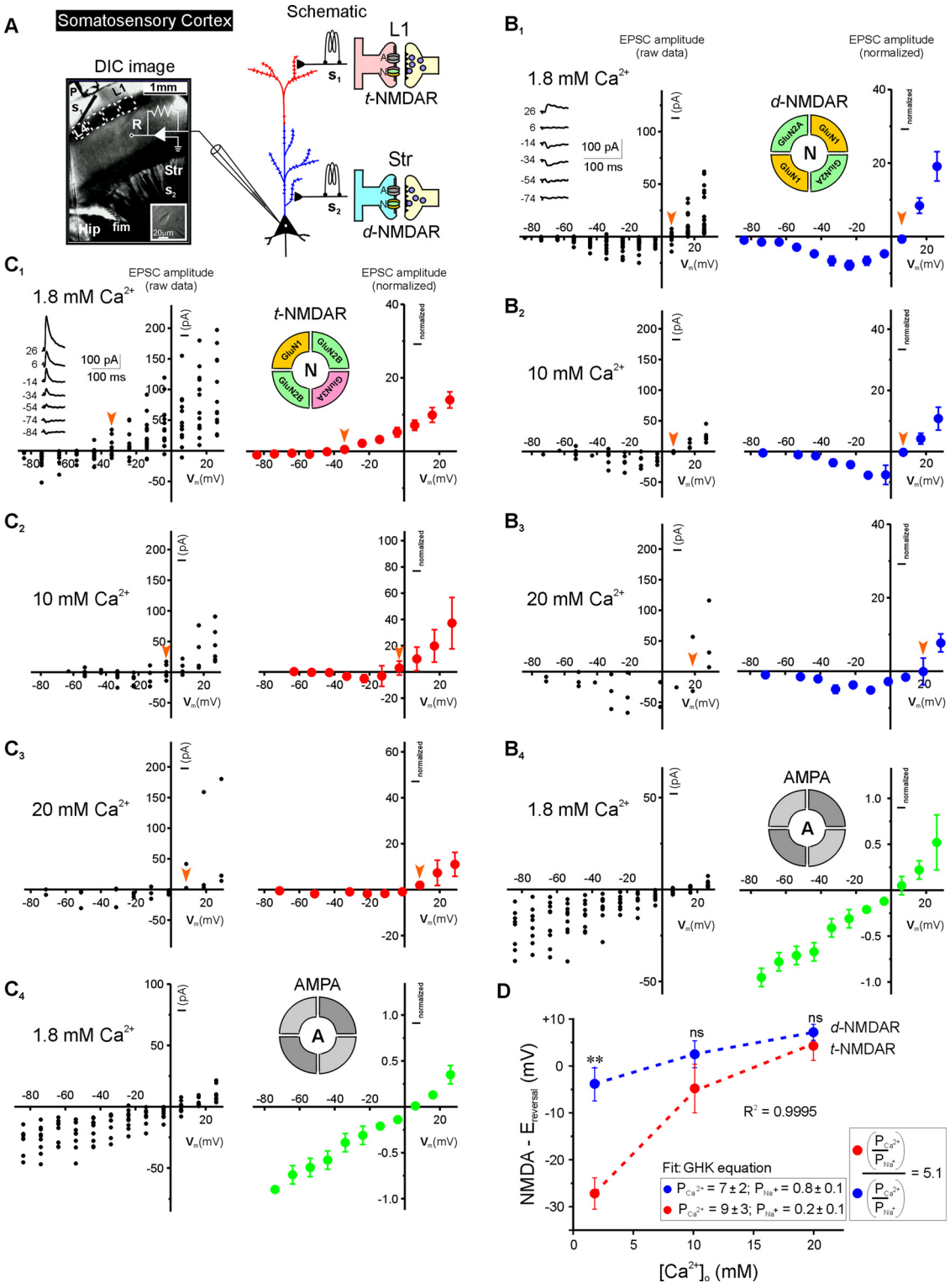

(caption on next page)

Differentiating t- and d-NMDAR mediated EPSCs in brain tissue

Synaptic *t*-NMDARs are distinguished from *d*-NMDARs in brain slices (Figs. 1, 2) by the current-voltage relationship profile (*I–V*) of their excitatory postsynaptic currents (EPSCs), decay kinetics and antagonism with D-serine and/or D-AP5 (Beesley et al., 2019; Pilli and Kumar, 2012, 2014). Whole-cell voltage-clamp recordings are made from visually identified pyramidal neurons in a region of interest (Figs. 1A, 2A1) in response to minimal stimulation of local afferents. The evoked EPSCs are dissected pharmacologically to isolate the NMDAR-mediated component from the AMPAR-mediated component using a cocktail of picrotoxin (PTX, 50 μM) and NBQX (10 μM) in either aCSF or HEPES-buffered Ringer's solution (ion substitution experiments) and confirmed through antagonism with D-AP5 (40 μM) (Fig. 2A2). The voltage-dependence of the pharmacologically-isolated NMDAR-mediated responses, measured using peak EPSC amplitudes at

Fig. 1. Assessment of Ca^{2+} permeability and selectivity in *t*- and *d*-NMDARs on pyramidal neurons (layer 5) of the somatosensory cortex using ion-substitution experiments. The data in this figure was obtained from an earlier study (Pilli and Kumar, 2012) and is being presented here for showcasing the differences and/or similarities between *t*-NMDAR properties between the somatosensory and entorhinal cortices. ***A***: electrophysiological recording in a thalamocortical slice preparation (*left*, differential interference contrast image) and schematic (*right*) of the placement of stimulating (S_1, S_2 for layer 1/L1 and striatal/Str stimulation respectively), local perfusion (P) and recording (R) electrodes in relation to the barrels (demarcated regions in layer 4), striatum (Str), and hippocampus (Hip). ***B-C***: current-voltage (*I-V*) relationships (raw data, *left*; normalized data, *right*) of the pharmacologically-isolated NMDA (N) and AMPA (A) receptor-mediated EPSCs evoked by concomitant alternate minimal-stimulation of Str (***B1-B4***) and L1 (***C1-C4***) inputs under (in mM) 1.8 (aCSF, *B1, C1*; *B4, C4*), 10 (*B2, C2*) and 20 (*B3, C3*) extracellular Ca^{2+} concentrations. Insets in B1 and C1 are representative sets of NMDAR-mediated EPSCs (averaged from ≥ 10 traces) at the indicated holding potentials (mV). A schematic of the putative subunit composition of the GluN2 subunit-containing di (*d, blue*) and GluN2 + GluN3 subunit-containing triheteromeric (*t, red*) NMDARs (*insets*) and their location at corresponding inputs shown color-coded along the dendrite. ***D***, Averaged shifts in reversal potential (E_{rev} in HEPES-buffered Ringer's solution, *red arrowheads*) of NMDAR-mediated EPSCs (measured from individual *I-Vs*) as a function of extracellular Ca^{2+} concentration for the respective pathways. Relative permeability of Ca^{2+} and Na^+ obtained from fits of data with the extended GHK constant-field equation (dashed lines; *R*, correlation coefficient) is shown in the boxed inset. Each point on the plots represents an ensemble average from a number of cells and error bars represent SEM, where this is greater than the size of the symbol. Statistical comparisons are between E_{rev} for NMDARs in the two pathways. $^{**}P < 0.01$; *ns* $P > 0.05$, *t*-test. (For interpretation of the references to colour in this figure legend, the reader is referred to the web version of this article).

various holding potentials in the range -84 to +26 mV (Figs. 1C1–C3, B1–B3; 2B1–B3, C1–C3), is used for determining rectification and reversal potential (E_{rev}). *t*-NMDAR-mediated synaptic currents have outwardly-rectifying *I–V* relationships with EPSCs reversing polarity at hyperpolarized holding potentials (Figs. 1C1, 2B1) compared with *d*-NMDARs that have prominent regions of negative slope and reverse polarity around 0 mV, the reversal potential for glutamate (Figs. 1B1, 2C1). The *t*-NMDAR-mediated EPSCs are AMPA-like with rapid decay kinetics and reduced affinity for Mg^{2+} unlike those mediated by *d*-NMDARs which are relatively much slower and blocked by Mg^{2+} at rest. While both *t*- and *d*-NMDAR responses are antagonized by the selective pan-NMDAR antagonist D-AP5, only *t*-NMDAR mediated EPSCs are antagonized by D-serine. We used these criteria to delineate *t*- from *d*-NMDAR-mediated synaptic currents in the somatosensory barrel cortex (Pilli and Kumar, 2012, 2014) and in the medial entorhinal area of the rat brain (Beesley et al., 2019).

Ca^{2+} permeability and selectivity in t- and d-NMDARs in the somatosensory cortex

To compare Ca^{2+} permeability in native *t*- versus *d*-NMDARs, we took advantage of receptors at layer (L)1/primary whisker-motor-cortex inputs onto L5 pyramidal neurons in somatosensory cortex that are triheteromeric assemblies of GluN1, GluN2B and GluN3A subunits, and those at thalamic/striatal (Str) inputs onto the same neurons that are diheteromeric, containing GluN1 and GluN2A subunits (Pilli and Kumar, 2012). The co-expression of these synaptic receptors in single neurons enabled a firsthand comparison of their properties under the more physiological setting of acute brain slices in which both inputs could be stimulated concomitantly while recording from individual neurons (Kumar and Huguenard, 2003) (Fig. 1A). If indeed GluN3-containing *t*-NMDARs at L1 inputs are selective for Ca^{2+} over Na^+, the *I–V* relationships of the pure, pharmacologically-isolated EPSCs would be expected to reverse polarity at hyperpolarized holding potentials, closer to the equilibrium potential for K^+ ($E_{eq,\ K+}$) and away from the equilibrium potential for Na^+ ($E_{eq,\ Na+}$), instead of ~ 0 mV, the reversal potential (E_{rev}) expected in *d*-NMDARs at Str inputs, established jointly by Na^+ and K^+. The permeability of GluN3-containing *t*-NMDARs to Cl^- has not actually been assessed even though NMDARs have been suggested to be impermeable to it (Mayer and Westbrook, 1987; Sharma and Stevens, 1996). Although Ca^{2+} contributes minimally to E_{rev}, owing to the relatively smaller concentrations inside and outside neurons under normal physiological conditions, K^+ efflux through these receptors (outwardly rectifying current at hyperpolarized potentials) would be countered by Ca^{2+} influx ($E_{eq,\ Ca2+} > > 0$ mV). Additionally, *I–Vs* for NMDARs at L1 inputs would not be expected to display prominent regions of negative slope compared with Str inputs, owing to smaller Na^+-mediated inward currents. Finally, because ion selectivity is not necessarily correlated with ion permeability, best exemplified by the NMDAR's voltage-dependent Mg^{2+} blockade, the hyperpolarized E_{rev} of GluN3-containing *t*-NMDARs at L1 inputs would be expected to either remain invariant or shift in the positive direction (towards $E_{eq,\ Ca2+}$) upon elevation of extracellular Ca^{2+}, if these receptors are to be deemed Ca^{2+} permeable (Ascher and Nowak, 1988; Mayer and Westbrook, 1987).

Indeed, unlike NMDAR-mediated EPSCs at Str inputs whose *I–Vs* reversed polarity close to 0 mV (5.1 ± 0.6 mV, n = 23 cells, aCSF; Fig. 1B1) and displayed prominent regions of negative slope (Fig. 1B1–B3), NMDAR-mediated EPSCs at L1 inputs consistently reversed polarity at a significantly hyperpolarized holding potential (−35 ± 4 mV, n = 12 cells, aCSF; $p < 0.01$, *t*-test; Fig. 1C1) and were characterized by outwardly-rectifying *I–Vs* (Fig. 1C1–C3). Recording conditions were optimal for making these measurements as *I–Vs* for the pure, pharmacologically-isolated AMPAR-mediated components at both inputs were linear as expected with EPSCs reversing polarity close to 0 mV (5.4 ± 2.8 mV for Str inputs and 4.1 ± 3.0 mV for L1, n = 13 cells, aCSF; $p = 0.8$, *t*-test; Fig. 1B4, C4). Upon isosmotic elevations in extracellular Ca^{2+} from 1.8 mM (similar to aCSF) to 10 mM and subsequently to 20 mM, E_{rev} shifted in a positive direction for both Str (-3.8 mV → 2.5 mV → 7.2 mV; $p = 0.2$, repeated-measures ANOVA; Fig. 1B2–B3) and L1 inputs (−27.2 mV → -4.8 mV → 4.3 mV; $p < 0.05$, repeated-measures ANOVA; Fig. 1C2–C3). The shifts in E_{rev} were overall greater for L1 compared to the Str EPSCs, with maximal change occurring in L1 during transition from 1.8 mM to 10 mM (Fig. 1D). While the permeability of divalent Ca^{2+} ($P_{Ca}{}^{2+}$) relative to monovalent Cs^+ ($P_{Cs}{}^+$ assumed 1), estimated through optimal fits of the data using the extended GHK constant-field equation (Mayer ML and Westbrook GL, 1987), for NMDARs at L1 inputs was similar to $P_{Ca}{}^{2+}$ for NMDARs at Str inputs (9 ± 3 vs. 7 ± 2 respectively; $p = 0.6$, *t*-test; n = 6 cells), the relative permeability of Na^+ ($P_{Na}{}^+$, kept a free parameter) for the same receptors at L1 inputs was significantly smaller than $P_{Na}{}^+$ for receptors at Str inputs (0.2 ± 0.1 vs. 0.8 ± 0.1 respectively; $p < 0.005$, *t*-test). Thus, relative to Na^+, the GluN1, GluN2B and GluN3A containing *t*-NMDARs at L1 inputs are ~5-fold more permeable to Ca^{2+} than the GluN1/GluN2A-containing NMDARs at Str inputs ($P_{Ca}{}^{2+}/P_{Na}{}^+$ or the fractional Ca^{2+} current (Schneggenburger et al., 1993), for L1 ≥ $P_{Ca}{}^{2+}/P_{Na}{}^+$ for Str). Additionally, these data confirm that GluN3 containing *t*-NMDARs at L1 inputs are not only permeable to Ca^{2+}, they are selective for Ca^{2+} over Na^+ ($0 < P_{Na}{}^+ < < 1$), as corroborated by the hyperpolarized non-zero E_{rev} of their EPSCs, in contrast with the non-GluN3 containing *d*-NMDARs at Str inputs.

Ca^{2+} permeability and selectivity in t- and d-NMDARs in the entorhinal cortex

While the somatosensory cortex highlighted input-specific differences in ion selectivity between *t*- and *d*-NMDARs, we tested the generality of these observations in the medial entorhinal area (MEA, Fig. 2A1) where L3 pyramidal neurons could be segregated into those

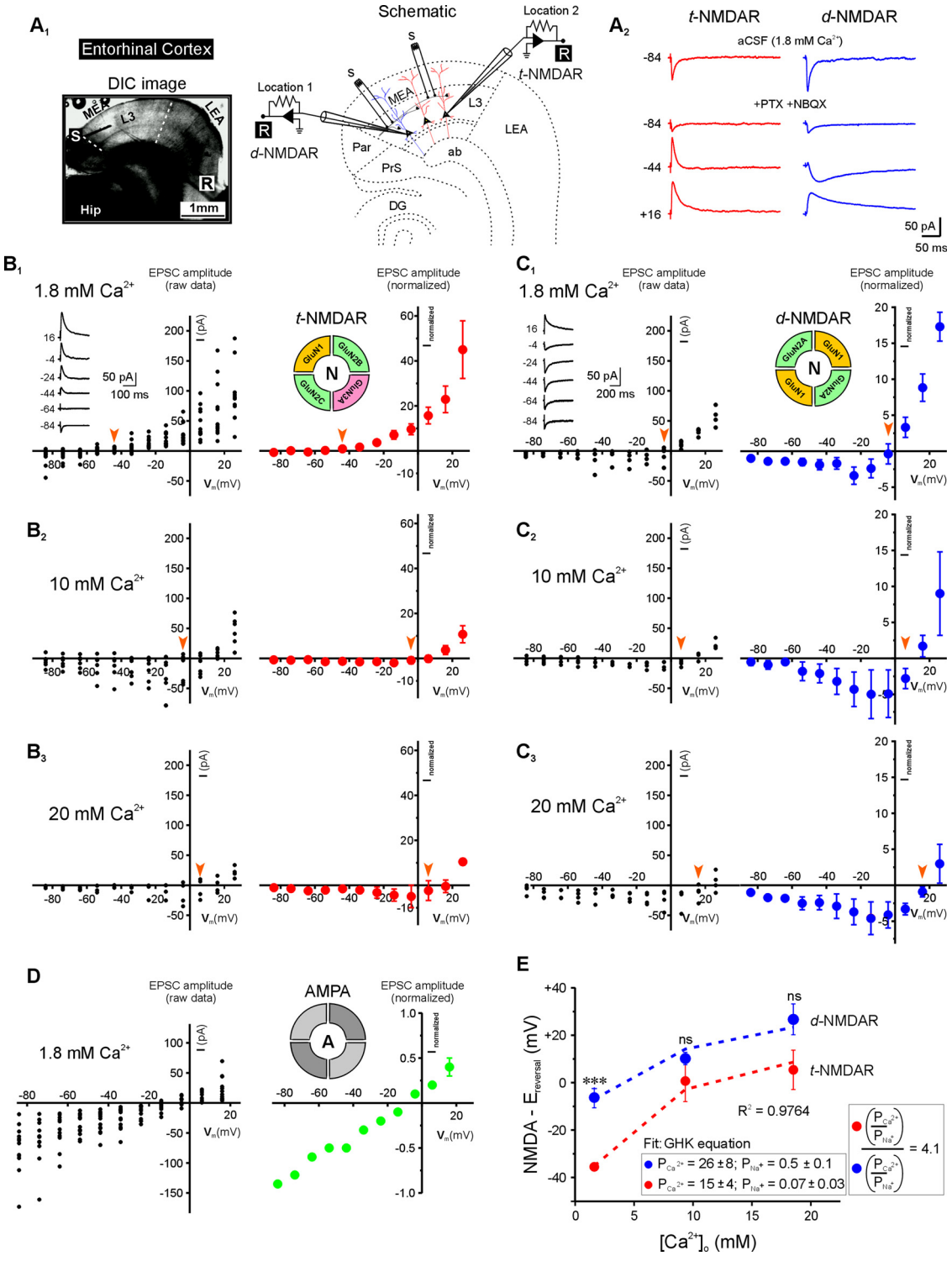

(caption on next page)

that expressed *d*-NMDARs alone (occupy medial portions of the MEA, juxtaposed with the presubiculum and parasubiculum) and those that expressed both receptor subtypes (spread throughout the bulk of the MEA) (Beesley et al., 2019). These neurons could be distinguished from one another based on the directionality of their pharmacologically-isolated NMDAR-mediated EPSCs when depolarized from rest (say to a holding potential of -44 mV) and by their decay kinetics (Fig. 2A2). Accordingly, the *I–Vs* were outwardly rectifying in ~80 % of neurons assayed, indicating expression of GluN1/GluN2/GluN3-containing *t*-NMDARs (Fig. 2B1–B3), and of the conventional type, reversing close to 0 mV with prominent regions of negative slope, in rest of the neurons sampled (~20 %), indicating expression of GluN1/GluN2-containing *d*-NMDARs (Fig. 2C1–C3). Blocking *t*-NMDARs in neurons with outwardly rectifying *I–Vs* pharmacologically, with D-serine for example, unmasked *d*-NMDARs, with all responses antagonized using D-AP5 (Beesley et al., 2019). Unlike the somatosensory cortex however, pyramidal neurons in MEA did not show any pathway specify differences in properties of NMDAR-mediated EPSCs which were uniform throughout

Fig. 2. Assessment of Ca^{2+} permeability and selectivity in NMDARs on pyramidal neurons (layer 3) of the medial entorhinal cortex (MEA) using ion-substitution experiments. Portions of the data in this figure were obtained from an earlier study (Beesley et al., 2019) and are being presented here for showcasing the differences and/or similarities between *t*-NMDAR properties between the somatosensory and entorhinal cortices. ***A1-A2***: electrophysiological recording from neurons expressing GluN2 subunit-containing *d*-NMDARs (*location 1*) and GluN2 + GluN3 subunit-containing *t*-NMDARs (*location 2*) in a horizontal slice preparation (*left*) and schematic (*right*) of the placement of stimulating (S) and recording (R) electrodes at the two locations within MEA (demarcations shown separate the medial and lateral portions of the entorhinal area; A1). Traces (*right panel*) are averaged EPSCs recorded in the two neuron types under the indicated conditions shown here to illustrate directionality of currents and kinetic changes during the sequence of manipulations leading up to the holding potential of +16 mV (A2) ***B-D***: current-voltage (*I-V*) relationships (raw data, *left*; normalized data, *right*) of the pharmacologically-isolated NMDA (N) and AMPA (A) receptor-mediated EPSCs evoked by minimal stimulation of local afferents at recording locations 2 (***B1-B4***) and 1 (***C1-C4***) under (in mM) 1.8 (aCSF, *B1, C1*; *D*), 10 (*B2, C2*) and 20 (*B3, C3*) extracellular Ca^{2+} concentrations. Insets in B1 and C1 are representative sets of NMDAR-mediated EPSCs (averaged from ≥ 10 traces) at the indicated holding potentials (mV). A schematic of the putative subunit composition of the di (*d*, *blue*) and triheteromeric (*t*, *red*) NMDARs (*insets*) is shown color-coded depending on their location within MEA. ***E***, Averaged shifts in reversal potential (E_{rev} in HEPES-buffered Ringer's solution, *red arrowheads*) of NMDAR-mediated EPSCs (measured from individual *I-Vs*), as a function of extracellular Ca^{2+} concentration for two neuron types. Relative permeability of Ca^{2+} and Na^{+} obtained from fits of data with the extended GHK constant-field equation (dashed lines; *R*, correlation coefficient) is shown in the boxed inset. Each point on the plots represents an ensemble average from a number of cells and error bars represent SEM, where this is greater than the size of the symbol. Statistical comparisons are between E_{rev} for NMDARs in the two locations. ***$P < 0.0001$; *ns* $P > 0.05$, *t*-test. (For interpretation of the references to colour in this figure legend, the reader is referred to the web version of this article).

each of the two distinct populations (*I–Vs* evoked by on- or off-column stimulation between L1 and L3 remained invariant). Only the *t*-NMDAR containing neurons showed the atypical hyperpolarized E_{rev} (-69 ± 3 mV, n = 14 cells, aCSF; Fig. 2B1) but not those containing *d*-NMDARs (E_{rev} ~0 mV, n = 4 cells, aCSF; Fig. 2C1). Furthermore, *I–Vs* for the pharmacologically-isolated AMPAR-mediated component in these neurons were linear with EPSCs reversing polarity close to 0 mV (−7 ± 2 mV, n = 12 cells, aCSF; Fig. 1D). Although shifts in E_{rev} to positive potentials were observed in both neuron types, upon isosmotic elevations in extracellular Ca^{2+} from 1.8 mM to 10 mM and subsequently to 20 mM (GluN3-containing: −36 mV → 0.7 mV →5.4 mV; GluN3-lacking: −6.3 mV → 10.2 mV → 26.7 mV; $p < 0.01$ for both, repeated-measures ANOVA; Fig. 2B2–B3; C2–C3), they were overall greater for the *t*-NMDAR containing neurons compared with those containing *d*-NMDARs alone (Fig. 2E). The P_{Ca}^{2+} estimated for NMDARs in the MEA were larger than in the somatosensory cortex, likely on account of the number of receptors at these inputs, but not dissimilar between the GluN3-containing *t*-NMDARs and the non-GluN3-containing *d*-NMDARs (15 ± 4 vs. 26 ± 8 respectively; $p = 0.2$, *t*-test; n = 6 and 4 cells respectively; Fig. 2E). In contrast, P_{Na}^{+} for GluN3-containing *t*-NMDARs was significantly smaller than P_{Na}^{+} for the non-GluN3-containing *d*-NMDARs (0.07 ± 0.03 vs. 0.5 ± 0.1 respectively; $p < 0.005$, *t*-test). Thus, relative to Na^{+}, the GluN3-containing *t*-NMDARs were at least 4-fold more permeable to Ca^{2+} than the non-GluN3-containing *d*-NMDARs (P_{Ca}^{2+}/P_{Na}^{+} or the fractional Ca^{2+} current for GluN3-conaining NMDARs > P_{Ca}^{2+}/P_{Na}^{+} for non-GluN3-containing NMDARs) and were selective for Ca^{2+} over Na^{+} ($0 < P_{Na}^{+} << 1$). Indeed, influx of excess Ca^{2+} can be excitotoxic to cells and L3 neurons in the MEA belong to a vulnerable population of neurons that are known to perish under conditions of hyperexcitability – hallmark pathology of Temporal Lobe Epilepsy (Du et al., 1995; Kumar and Buckmaster, 2006).

Discussion

This study assessed Ca^{2+} permeability and selectivity of native *t*- and *d*-NMDARs at the cell- and input-specific levels in the entorhinal and somatosensory cortices. The data suggests that *t*-NMDARs are four to five-fold more Ca^{2+} permeable than *d*-NMDARs. This increased permeability to Ca^{2+}could be accounted for by the GluN3 subunit which endows these receptors with the ability to select for Ca^{2+} over Na^{+}. Many of the features that enable their distinction from *d*-NMDARs, including the hyperpolarized reversals and outward rectification of their EPSCs can be explained through GluN3-mediated ion selectivity. In this regard, the extended GHK constant-field equation (Mayer and Westbrook, 1987) dovetails well with ion-substitution experiments for assessments of Na^{+}/Ca^{2+} permeability and selectivity of synaptic NMDARs in brain tissue.

This study also highlights the contribution of individual subunits and their subtypes in shaping NMDAR function in different brain regions. In the somatosensory cortex for example, we have shown that potentiating paradigms for convergent inputs onto single neurons can be distinct and that synapse-specific enhancements in efficacy are tuned to specific temporal patterns of synaptic activity and the subunit composition of underlying NMDARs. Thus, while delta burst stimulation (0.1–4 Hz) was found to be most efficacious at potentiating *t*-NMDAR-containing synapses at L1 inputs, theta burst stimulation (4–7 Hz) was determined to be most efficacious at potentiating *d*-NMDAR-containing synapses at Str inputs within the same neuron, highlighting the role of the GluN2 and GluN3 subunits in mediating Ca^{2+}-dependent synaptic plasticity (Pilli J and Kumar SS, 2014). The Co-expression of *t*- and *d*-NMDARs at individual inputs onto neurons in the entorhinal cortex might therefore enable them to integrate or encode distinct patterns or information through single synapses (Beesley et al., 2019). In a related study in the agranular frontal cortex for example, we showed that pathway specific differences in the GluN2 subunit of NMDARs at callosal and intracortical inputs onto pyramidal neurons accounted for whether the receptors would favor synaptic integration or coincident detection. Thus, GluN2B-containing NMDARs at intracortical inputs, by virtue of their slower decay kinetics, would be amenable to synaptic integration in contrast with the GluN2A-containing NMDARs at callosal inputs which by virtue of their faster decay kinetics would be amenable to coincident detection, thereby highlighting the role of GluN2 subtypes in NMDAR-mediated processing of synaptic information (Kumar and Huguenard, 2003). In addition to differences in kinetic properties, these receptors also showed differences in voltage-dependent properties including the affinity with which they bound Mg^{2+}. However, their *I–Vs* resembled those of *d*-NMDARs in the somatosensory cortex, reversing close to 0 mV with prominent regions of negative slope, indicating the absence of the GluN3 subunit and by extension, the ability to screen cations.

Thus, while all NMDAR subunits offer substrates for binding ligand or co-agonist (among a host of other molecules including Zn^{2+}, a co-factor) for optimal receptor function, they appear to have distinct regulatory roles. The GluN1 subunit binds glycine and is responsible for dimerization and activation of the NMDAR and therefore considered mandatory in putting a functional receptor together (Benveniste and Mayer, 1991). The GluN2 subunits offer binding sites for glutamate and regulate receptor kinetics via ion channel gating, deactivation and desensitization, which determine the time course of NMDAR-mediated synaptic currents (Clements and Westbrook, 1991). The GluN1 and GluN2 subunits together facilitate the permeability of Na^{+}, K^{+} and Ca^{2+} through the NMDAR. The GluN3 subunits bind glycine and together with GluN1 make glycine activated NMDARs that have reduced Ca^{2+}-permeability (Chatterton et al., 2002; Das et al., 1998). We believe that the GluN3 subunit can replace one of the glycine-binding GluN1 subunits and combine with GluN2 subunits to give rise to glutamate-activated *t*-NMDARs in native tissue (Beesley et al., 2019;

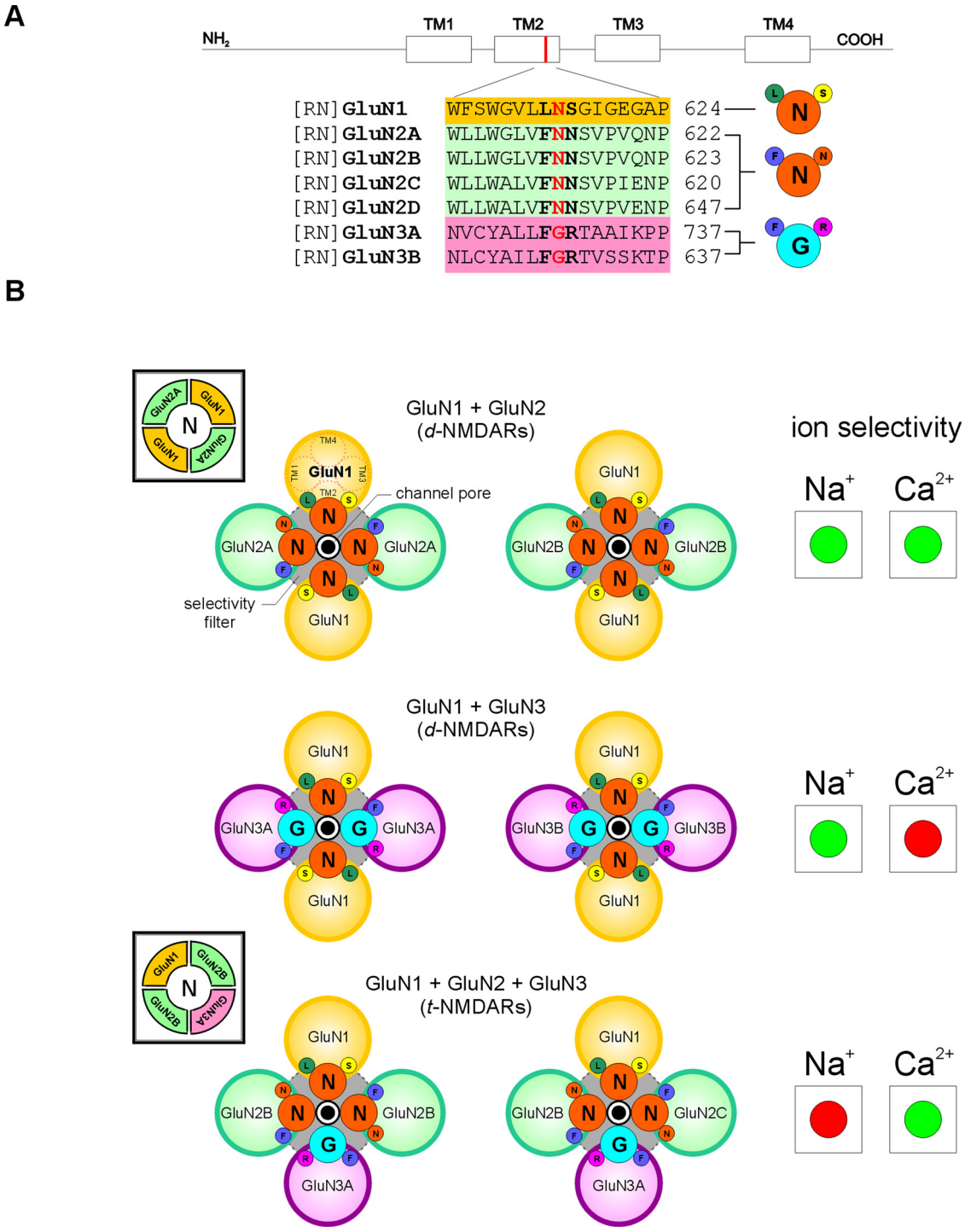

Fig. 3. Ion selectivity in di- and triheteromeric NMDARs is dependent on the combination of receptor subunits and ultimately on the sequence of amino acids that compose the selectivity filters in the pore-forming region of the receptor channels. ***A***, NMDAR subunits with predicted transmembrane (TM) regions and TM2 sequence alignment of GluN1; GluN2A, 2B, 2C, 2D; GluN 3A, 3B from rat (RN, *rattus norvegicus*). Amino acid residues determining functional channel properties are indicated in bold and conserved residues determining ion selectivity in red. Numbers refer to amino acid positions within subunits. Abbreviations for the amino acid residues are: A, Ala; C, Cys; E, Glu; F, Phe; G, Gly; I, Ile; K, Lys; L, Leu; N, Asn; P, Pro; Q, Gln; R, Arg; S, Ser; T, Thr; V, Val; W, Trp; and Y, Tyr. ***B***, Schematic arrangement of subunits and amino acid residues that constitute the putative selectivity filters in GluN3-containing/non-containing di- and triheteromeric NMDARs (*left*), and their selectivity (enhanced, green; diminished, red) for Na^+ and/or Ca^{2+} ions (*right*). (For interpretation of the references to colour in this figure legend, the reader is referred to the web version of this article).

Kumar, 2016; Pilli and Kumar, 2012, 2014; Tong et al., 2008). Incorporation of the GluN3 subunit in this case not only speeds up the decay kinetics of NMDAR-mediated EPSCs but, as demonstrated through this and prior studies, broadens their dynamic range, fine tunes their activation to specific patterns of neuronal activity for plasticity (Pilli and Kumar, 2014) and importantly, enhances Ca^{2+} permeability by incorporating cation selectivity. Can differences in function between these NMDAR subtypes be accounted for by differences in structure?

Correlating structure with function of t-NMDARs

Site directed mutagenesis of amino acid residues within the pore-forming TM2 domains of GluN1 and GluN2 subunits of heterologously expressed *d*-NMDARs shows that cation permeability, especially of divalent Ca^{2+}, is mediated by asparagine at location 598 in GluN1 (N598) (Burnashev et al., 1992b; Monyer et al., 1994; Moriyoshi et al., 1991), the mandatory subunit, and this residue is conserved at homologous positions within all members of the GluN2 subunit family (GluN2A-2D; Fig. 3A). Together, these residues constitute the putative selectivity filter that enables permeation of both Na^+ and Ca^{2+} ions through these receptor channels (Fig. 3B). GluN3 subunits (3A and 3B), unlike GluN2, have glycine / arginine instead of asparagine at homologous positions within their TM2 domains (Fig. 3A). Expression of GluN1 and GluN3 subunits in *Xenopus* oocytes, HEK cells and juvenile hippocampal slices yields *d*-NMDARs that are activated by glycine instead of glutamate (Chatterton et al., 2002; Grand et al., 2018) and relatively Ca^{2+}-impermeable (Chatterton et al., 2002; Matsuda et al., 2002) cf. (Otsu et al., 2019) even in combination with GluN2 (Perez-Otano et al., 2001). The incorporation of GluN3A in the subunit composition of diheteromeric GluN1/GluN2B-containing NMDARs, on the other hand, causes a ~5 to 10-fold reduction in NMDA-evoked Na^+ current in oocytes (Sucher et al., 1995) consistent with what we see in native *t*-NMDARs. However, there is a need for caution in interpreting receptor function across various platforms because co-injection of NR3A with NR1/NR2 subunits in cell expression systems has been reported to yield NMDARs with decreased unitary conductance and Ca^{2+} permeability that is recapitulated in acutely isolated cortical neurons from very young (postnatal day 8) wild-type mice (Sasaki et al., 2002). Our data from synaptic NMDARs in intact brain slices across different regions suggest that without GluN3 there is no control over selectivity of either monovalent (i.e. Na^+) or divalent (i.e. Ca^{2+}) cations (GluN3-containing *d*-NMDARs however appear to prefer Na^+ over Ca^{2+}). This situation is altered with the incorporation of GluN3 to make *t*-NMDARs, which acquire selectivity for Ca^{2+} over Na^+ (Fig. 3B).

Dual regulation of monovalent and divalent cations in *t*-NMDARs is possible through ion selectivity (Premkumar and Auerbach, 1996; Schneggenburger, 1998) alone, or in combination with pore-size/conductance-based screening of ions (Burnashev et al., 1992b; Hille, 2001; Wollmuth et al., 1996). Given the data from electrophysiological and/or ion-substitution experiments in the frontal, somatosensory and entorhinal cortices, together with the fact that unsolvated Na^+ and Ca^{2+} ions are comparable in size (Shannon, 1976) (Fig. 4A), suggests that the increased permeability to Ca^{2+} and decreased permeability to Na^+ in *t*-NMDARs arises primarily from GluN3-mediated cation selectivity. Subunit-dependent ion-selectivity represents a previously unrealized mechanism for finer control of Ca^{2+} influx, enhancing the repertoire of synaptic NMDARs. Given that influx of ions through *t*-NMDARs is predominantly Ca^{2+}, despite the high extracellular sodium-to-calcium ratio ($[Na^+]_o$: $[Ca^{2+}]_o$ is ~100:1; Fig. 4B1), suggests severe selection against monovalent ions at the synapse. On the other hand, the high intracellular potassium-to-calcium ratio ($[K^+]_i$: $[Ca^{2+}]_i$ is ~100:1; Fig. 4B1) suggests that discrimination against K^+ ions is low (3000:1) and that reversal potential in these receptors is dominated by $[K^+]_i$ rather than $[Ca^{2+}]_i$ (Hille, 2001), and consistent with the hyperpolarized E_{rev} observed in native *t*-NMDARs. Higher selectivity could facilitate increased permeability on account of the electrostatic repulsion of a monovalent cation by a divalent cation and the speeding-up of divalent cation flow when the channel becomes multiply occupied (Sharma and Stevens, 1996) (Fig. 4B2). Note that synaptic currents are smaller when extracellular concentration is raised in our ion-substitution experiments for reasons not well understood; however, a significant change in membrane potential occurs with the movement of very few ions– only 1 of every 100,000 K^+ must enter or leave the cell to change membrane potential by 100 mV (Silverthorn, 2016).

Ion selectivity in ligand-gated ion channels

Non-ligand gated ion channels have been studied extensively in the context of their role as nature's gatekeepers, allowing certain ions to traverse the membrane while excluding others, to control the electrical state of the cell (Zagotta, 2006). By comparison, ion selectivity in ligand-gated ionotropic receptors has remained underappreciated despite its potential to regulate activity-dependent processes, set thresholds for receptor-activation and directly influence the efficacy of synaptic transmission. Finer control of Ca^{2+} influx through NMDARs through ion-selectivity, for example, might mean the difference between Long-Tem Potentiation (LTP) and Long-Term Depression (LTD) and the ability to globally regulate synaptic plasticity (Liu et al., 2004; Nishiyama et al., 2000; Sheng et al., 1994). In this sense, GluN3-containing synaptic *t*-NMDARs have helped break the stereotype of NMDARs being nonselective to cations while prompting a closer look at subunit composition and the role of receptor subunits per se in regulating ion selectivity in ligand-gated ionotropic receptors. Subunit-mediated changes in ion-selectivity extends beyond NMDARs as seen in the closely related AMPARs which are impermeable to Ca^{2+} when assembled with the GluA2 subunit but become Ca^{2+} permeable without it (Hollmann et al., 1991; Kumar et al., 2002). Posttranscriptional modification of a glutamine residue to an arginine at the Q/R editing site in the putative selectivity filter underlies the subunits ability to modulate the permeability of various cations through these receptors (Burnashev et al., 1992a).

Despite the range in selectivity, from highly K^+-selective to highly Na^+- or Ca^{2+}-selective, cation-selective channels are structurally related and essentially thought to be variations on K^+ channels (Zagotta, 2006). The breakdown of a conserved signature sequence of amino acids (TVGYG) in the selectivity filters of highly K^+-selective channels enables the emergence of Na^+ and eventually, Ca^{2+} permeability in these channels which constitute a continuum of channel types with variable levels of K^+, Na^+ and Ca^{2+} selectivity. The empirically deduced schema for ion selectivity in these channels, hypothetically depicted with a "selectivity dial" (Fig. 4C, *left panel*), shows the channels (•) arranged along the periphery of a rotary knob marked with a channel-selector (▼), and three orthogonally oriented indicators (red) for readout of K^+, Na^+ and Ca^{2+} selectivity. Cation selectivity levels are graded, color-coded (white/non-colored regions indicate non-selective and/or impermeant), and strategically positioned around the dial to capture the dynamics of change in ion selectivity as the knob is rotated. Thus, it can be inferred that loss of K^+ selectivity is associated with the emergence of Ca^{2+} permeability (Zagotta, 2006) and conversely increases in Ca^{2+}selectivity come at the expense of corresponding decreases in Na^+ permeability. We queried if this schema for cation selectivity in non-ligand gated ion channels extended to ligand gated AMPA and NMDA receptors (Fig. 4C, *right panel*) and whether it could reconcile the subunit-specific differences in cation selectivity observed via physiology. We find that most, if not all, known types of glutamatergic receptors fit the schema for ion selectivity in non-ligand gated ion channels including, but not restricted to GluN3-containing synaptic *t*-NMDARs (Beesley et al., 2019; Pilli and Kumar, 2012). This suggests that evolutionarily conserved principles of cation selectivity in ion channels transcend the distinction of whether they are ligand-gated or not. Subunit-mediated alterations in ion selectivity enable synaptic NMDARs to regulate Ca^{2+} influx relative to Na^+ - a nuance with potentially far reaching functional implications covering the gamut from synaptic plasticity to cell death.

Ethics comment

We have read and abided by all ethical standards for manuscripts submitted to IBRO reports.

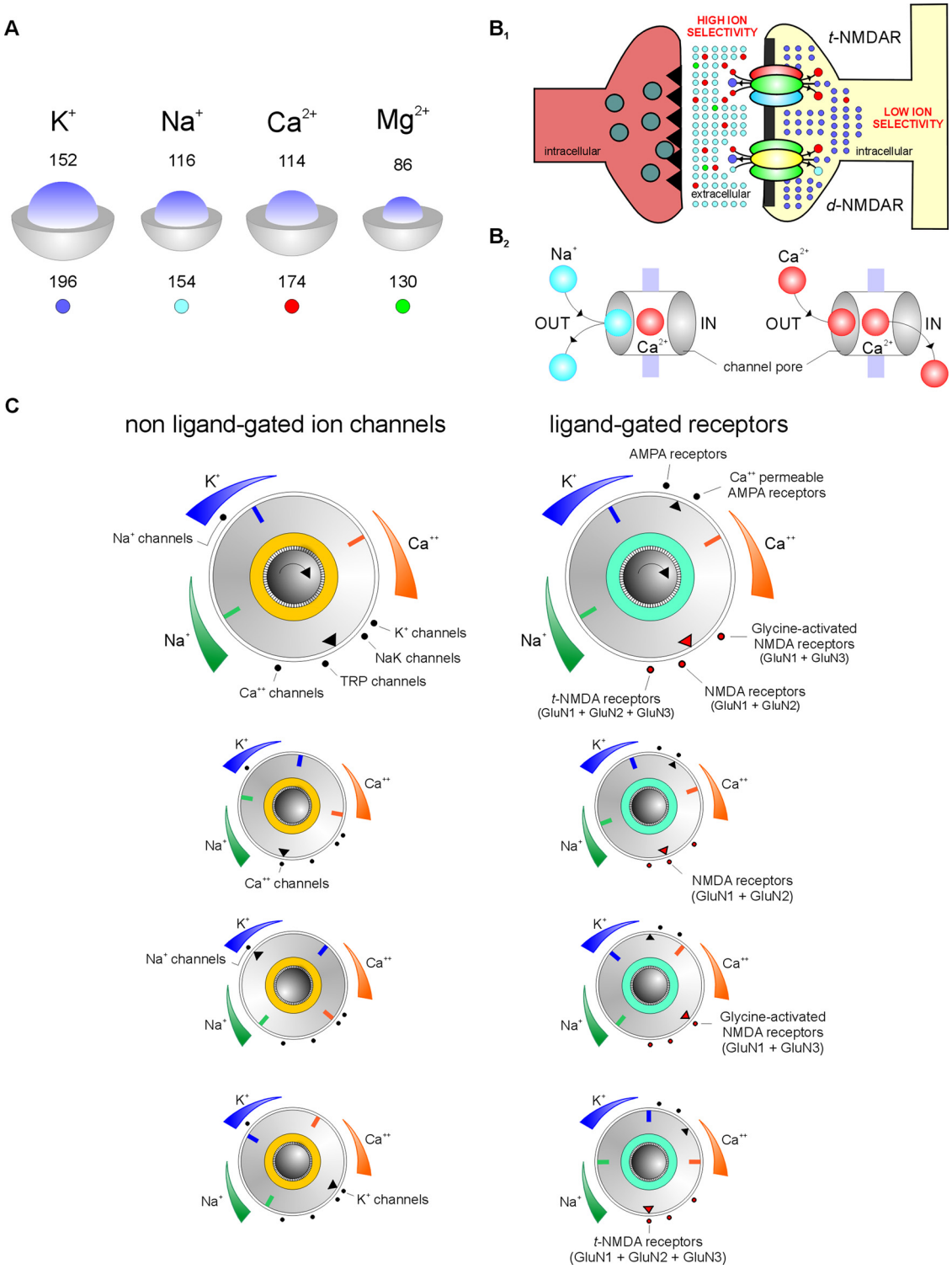

Fig. 4. Factors affecting permeability and selectivity within receptor channels include among others, (***A***) the relative size of ions (blue, *top number*) / atoms (gray, *bottom number*), where numbers indicate radii in picometers; and (***B***) their distribution within the intracellular and extracellular compartments of the postsynaptic element in which selectivity of ions differs significantly. *Inset* schematic showing how selectivity for Ca^{2+} influences its permeability. Note that we do not know what the dwell time for Ca^{2+} is within the pore of receptor channel. Schema for cation selectivity within non-ligand gated ion channels (***C, left panel***) and ionotropic glutamate receptors (***C, right panel***) with related examples. The rotary knob (center) is marked with a channel-selector (▼) and three orthogonally-oriented indicators (red) for read out of K^+, Na^+ and Ca^{2+} selectivity in selected channels (•) arranged along the periphery of a selectivity dial. Cation selectivity levels are graded (high ↔ low) and color-coded (non-colored regions indicate non-selective and/or impermeance). Note that emergence of Ca^{2+}/Na^+ selectivity entails loss of K^+ selectivity in both non-ligand gated ion channels and ligand-gated AMPA and NMDA receptors. However, lack of ion selectivity does not necessarily mean lack of ion permeability. (For interpretation of the references to colour in this figure legend, the reader is referred to the web version of this article).

Conflict of interest

None.

CRediT authorship contribution statement

Stephen Beesley: Methodology, Project administration. **Sanjay S. Kumar:** Conceptualization, Methodology, Project administration, Funding acquisition.

Acknowledgments

We wish to thank Dr. Jyotsna Pilli for her efforts in getting this project started and for her guidance.

This work was supported in part by grants from the CRC and CoM at Florida State University, Epilepsy Foundation, and the National Institutes of Health.

References

Ascher, P., Nowak, L., 1988. The role of divalent cations in the N-methyl-D-aspartate responses of mouse central neurones in culture. J. Physiol. 399, 247–266.
Beesley, S., Sullenberger, T., Pilli, J., Abbasi, S., Gunjan, A., Kumar, S.S., 2019. Colocalization of distinct NMDA receptor subtypes at excitatory synapses in the entorhinal cortex. J. Neurophysiol. 121, 238–254.
Benveniste, M., Mayer, M.L., 1991. Kinetic analysis of antagonist action at N-methyl-D-aspartic acid receptors. Two binding sites each for glutamate and glycine. Biophys. J. 59, 560–573.
Burnashev, N., Monyer, H., Seeburg, P.H., Sakmann, B., 1992a. Divalent ion permeability of AMPA receptor channels is dominated by the edited form of a single subunit. Neuron 8, 189–198.
Burnashev, N., Schoepfer, R., Monyer, H., Ruppersberg, J.P., Gunther, W., Seeburg, P.H., Sakmann, B., 1992b. Control by asparagine residues of calcium permeability and magnesium blockade in the NMDA receptor. Science 257, 1415–1419.
Chatterton, J.E., Awobuluyi, M., Premkumar, L.S., Takahashi, H., Talantova, M., Shin, Y., Cui, J., Tu, S., et al., 2002. Excitatory glycine receptors containing the NR3 family of NMDA receptor subunits. Nature 415, 793–798.
Chazot, P.L., Stephenson, F.A., 1997. Molecular dissection of native mammalian forebrain NMDA receptors containing the NR1 C2 exon: direct demonstration of NMDA receptors comprising NR1, NR2A, and NR2B subunits within the same complex. J. Neurochem. 69, 2138–2144.
Clements, J.D., Westbrook, G.L., 1991. Activation kinetics reveal the number of glutamate and glycine binding sites on the N-methyl-D-aspartate receptor. Neuron 7, 605–613.
Collingridge, G., 1987. Synaptic plasticity. The role of NMDA receptors in learning and memory. Nature 330, 604–605.
Cull-Candy, S., Brickley, S., Farrant, M., 2001. NMDA receptor subunits: diversity, development and disease. Curr. Opin. Neurobiol. 11, 327–335.
Cummings, K.A., Belin, S., Popescu, G.K., 2017. Residues in the GluN1 C-terminal domain control kinetics and pharmacology of GluN1/GluN3A N-methyl-d-aspartate receptors. Neuropharmacology 119, 40–47.
Das, S., Sasaki, Y.F., Rothe, T., Premkumar, L.S., Takasu, M., Crandall, J.E., Dikkes, P., Conner, D.A., et al., 1998. Increased NMDA current and spine density in mice lacking the NMDA receptor subunit NR3A. Nature 393, 377–381.
Dingledine, R., Borges, K., Bowie, D., Traynelis, S.F., 1999. The glutamate receptor ion channels. Pharmacol. Rev. 51, 7–61.
Du, F., Eid, T., Lothman, E.W., Kohler, C., Schwarcz, R., 1995. Preferential neuronal loss in layer III of the medial entorhinal cortex in rat models of temporal lobe epilepsy. J. Neurosci. 15, 6301–6313.
Grand, T., Abi Gerges, S., David, M., Diana, M.A., Paoletti, P., 2018. Unmasking GluN1/GluN3A excitatory glycine NMDA receptors. Nat. Commun. 9, 4769.
Hatton, C.J., Paoletti, P., 2005. Modulation of triheteromeric NMDA receptors by N-terminal domain ligands. Neuron 46, 261–274.
Hille, B., 2001. Ion Channels of Excitable Membranes. Sinauer., Sunderland, MA.
Hollmann, M., Hartley, M., Heinemann, S., 1991. Ca2+ permeability of KA-AMPA–gated glutamate receptor channels depends on subunit composition. Science 252, 851–853.
Kumar, S.S., 2016. Functional detection of novel triheteromeric NMDA receptors. In: Popescu, G.K. (Ed.), Ionotropic Glutamate Receptor Technologies. Springer, New York, pp. 71–80.
Kumar, S.S., Buckmaster, P.S., 2006. Hyperexcitability, interneurons, and loss of GABAergic synapses in entorhinal cortex in a model of temporal lobe epilepsy. J. Neurosci. 26, 4613–4623.
Kumar, S.S., Huguenard, J.R., 2003. Pathway-specific differences in subunit composition of synaptic NMDA receptors on pyramidal neurons in neocortex. J. Neurosci. 23, 10074–10083.
Kumar, S.S., Bacci, A., Kharazia, V., Huguenard, J.R., 2002. A developmental switch of AMPA receptor subunits in neocortical pyramidal neurons. J. Neurosci. 22, 3005–3015.
Liu, L., Wong, T.P., Pozza, M.F., Lingenhoehl, K., Wang, Y., Sheng, M., Auberson, Y.P., Wang, Y.T., 2004. Role of NMDA receptor subtypes in governing the direction of hippocampal synaptic plasticity. Science 304, 1021–1024.
Luo, J., Wang, Y., Yasuda, R.P., Dunah, A.W., Wolfe, B.B., 1997. The majority of N-methyl-D-aspartate receptor complexes in adult rat cerebral cortex contain at least three different subunits (NR1/NR2A/NR2B). Mol. Pharmacol. 51, 79–86.
Matsuda, K., Kamiya, Y., Matsuda, S., Yuzaki, M., 2002. Cloning and characterization of a novel NMDA receptor subunit NR3B: a dominant subunit that reduces calcium permeability. Brain Res. Mol. Brain Res. 100, 43–52.
Mayer, M.L., Westbrook, G.L., 1987. Permeation and block of N-methyl-D-aspartic acid receptor channels by divalent cations in mouse cultured central neurones. J. Physiol. (Paris) 394, 501–527.
Mayer, M.L., Westbrook, G.L., Guthrie, P.B., 1984. Voltage-dependent block by Mg2+ of NMDA responses in spinal cord neurones. Nature 309, 261–263.
McBain, C.J., Mayer, M.L., 1994. N-methyl-D-aspartic acid receptor structure and function. Physiol. Rev. 74, 723–760.
Monyer, H., Burnashev, N., Laurie, D.J., Sakmann, B., Seeburg, P.H., 1994. Developmental and regional expression in the rat brain and functional properties of four NMDA receptors. Neuron 12, 529–540.
Moriyoshi, K., Masu, M., Ishii, T., Shigemoto, R., Mizuno, N., Nakanishi, S., 1991. Molecular cloning and characterization of the rat NMDA receptor. Nature 354, 31–37.
Nishiyama, M., Hong, K., Mikoshiba, K., Poo, M.M., Kato, K., 2000. Calcium stores regulate the polarity and input specificity of synaptic modification. Nature 408, 584–588.
Otsu, Y., Darcq, E., Pietrajtis, K., Matyas, F., Schwartz, E., Bessaih, T., Abi Gerges, S., Rousseau, C.V., et al., 2019. Control of aversion by glycine-gated GluN1/GluN3A NMDA receptors in the adult medial habenula. Science 366, 250–254.
Perez-Otano, I., Schulteis, C.T., Contractor, A., Lipton, S.A., Trimmer, J.S., Sucher, N.J., Heinemann, S.F., 2001. Assembly with the NR1 subunit is required for surface expression of NR3A-containing NMDA receptors. J. Neurosci. 21, 1228–1237.
Pilli, J., Kumar, S.S., 2012. Triheteromeric N-methyl-d-aspartate receptors differentiate synaptic inputs onto pyramidal neurons in somatosensory cortex: Involvement of the GluN3A subunit. Neuroscience 222, 75–88.
Pilli, J., Kumar, S.S., 2014. Potentiation of convergent synaptic inputs onto pyramidal neurons in somatosensory cortex: dependence on brain wave frequencies and NMDA receptor subunit composition. Neuroscience 272, 271–285.
Pitzer, K.S., Mayorga, G., 1973. Thermodynamics of electrolytes. II. Activity and osmotic coefficients for strong electrolytes with one or both ions univalent. J. Phys. Chem. 77, 2300–2308.
Premkumar, L.S., Auerbach, A., 1996. Identification of a high affinity divalent cation binding site near the entrance of the NMDA receptor channel. Neuron 16, 869–880.
Sasaki, Y.F., Rothe, T., Premkumar, L.S., Das, S., Cui, J., Talantova, M.V., Wong, H.K., Gong, X., et al., 2002. Characterization and comparison of the NR3A subunit of the NMDA receptor in recombinant systems and primary cortical neurons. J. Neurophysiol. 87, 2052–2063.
Schneggenburger, R., 1998. Altered voltage dependence of fractional Ca2+ current in N-methyl-D-aspartate channel pore mutants with a decreased Ca2+ permeability. Biophys. J. 74, 1790–1794.
Schneggenburger, R., Zhou, Z., Konnerth, A., Neher, E., 1993. Fractional contribution of calcium to the cation current through glutamate receptor channels. Neuron 11, 133–143.
Shannon, R.D., 1976. Revised effective ionic-radii and systematic studies of interatomic distances in Halides and chalcogenides. Acta Crystallogr. Sect. A 32, 751–767.
Sharma, G., Stevens, C.F., 1996. Interactions between two divalent ion binding sites in N-methyl-D-aspartate receptor channels. Proc. Natl. Acad. Sci. U. S. A. 93, 14170–14175.
Sheng, M., Cummings, J., Roldan, L.A., Jan, Y.N., Jan, L.Y., 1994. Changing subunit composition of heteromeric NMDA receptors during development of rat cortex. Nature 368, 144–147.
Silverthorn, D.U., 2016. Human Physiology: An Integrated Approach. Paeson Education, Inc., USA.
Sucher, N.J., Akbarian, S., Chi, C.L., Leclerc, C.L., Awobuluyi, M., Deitcher, D.L., Wu, M.K., Yuan, J.P., et al., 1995. Developmental and regional expression pattern of a novel NMDA receptor-like subunit (NMDAR-L) in the rodent brain. J. Neurosci. 15, 6509–6520.
Sun, W., Hansen, K.B., Jahr, C.E., 2017. Allosteric interactions between NMDA receptor subunits shape the developmental shift in channel properties. Neuron 94 (58–64), e53.
Tong, G., Takahashi, H., Tu, S., Shin, Y., Talantova, M., Zago, W., Xia, P., Nie, Z., et al., 2008. Modulation of NMDA receptor properties and synaptic transmission by the NR3A subunit in mouse hippocampal and cerebrocortical neurons. J. Neurophysiol. 99, 122–132.
Tovar, K.R., McGinley, M.J., Westbrook, G.L., 2013. Triheteromeric NMDA receptors at hippocampal synapses. J. Neurosci. 33, 9150–9160.
Verdoorn, T.A., Burnashev, N., Monyer, H., Seeburg, P.H., Sakmann, B., 1991. Structural determinants of ion flow through recombinant glutamate receptor channels. Science 252, 1715–1718.
Wollmuth, L.P., Kuner, T., Seeburg, P.H., Sakmann, B., 1996. Differential contribution of the NR1- and NR2A-subunits to the selectivity filter of recombinant NMDA receptor channels. J. Physiol. 491 (Pt 3), 779–797.
Zagotta, W.N., 2006. Membrane biology: permutations of permeability. Nature 440, 427–429.